IEEE JOURNAL OF

QUANTUM ELECTRONICS

MARCH 1989 VOLUME 25 NUMBER 3 (ISSN 0018-9197)

A PUBLICATION OF THE IEEE LASERS AND ELECTRO-OPTICS SOCIETY

SPECIAL ISSUE ON NONLINEAR OPTICAL PHASE CONJUGATION

ANNOUNCEMENTS

Special Issue on Lasers in Biology and Medicine 243
Special Issue on Ultrafast Phenomena 244

QUANTUM ELECTRONICS LETTERS

RF-Excited Tunable CO Laser with Opto-Hertzian Frequency Stabilization ..... *G. N. Pearson and D. R. Hall* 245
Improved Coupled-Mode Theory of Anisotropic Optical Waveguides ..... *T. Feng, G. Feng, Y.-Z. Wu, and P.-D. Ye* 249
Electrooptic Diffraction Modulation in ZnO Film on Sapphire ..... *M.-S. Wu, T. Shiosaki, and A. Kawabata* 252

REGULAR PAPERS

Semiconductor Lasers

Efficient Frequency Noise Reduction of GaAlAs Semiconductor Lasers by Optical Feedback from an External High Finesse Resonator ..... *H. Li and H. R. Telle* 257
Optical Polarization Bistability in TM Wave Injected Semiconductor Lasers ..... *Y. Mori, J. Shibata, and T. Kajiwara* 265

Nonlinear Optics in Fibers

Theory of Stimulated Raman Scattering in Optical Fibers in the Pulse Walkoff Regime ..... *D. N. Christodoulides and R. I. Joseph* 273
Noise Characterization of Femtosecond Fiber Raman Soliton Lasers ..... *U. Keller, K. D. Li, M. Rodwell, and D. M. Bloom* 280

Other Papers

Criteria for Optical Bistability in a Lossy Saturating Fabry–Perot ..... *E. Garmire* 289
Matrix Formalism for Dispersive Laser Cavities ..... *O. E. Martínez* 296
Theoretical Investigation of an Integrated All-Optical Controller–Modulator Device Using QCSE in a Multiquantum Well Phototransistor ..... *S. Hong and J. Singh* 301

SPECIAL ISSUE PAPERS

Introduction to the Special Issue ..... *D. M. Pepper* 312

Propagation, Low-Level Signals, and Superresolution

Polarization and Spatial Information Recovery by Modal Dispersal and Phase Conjugation: Properties and Applications *(Invited Paper)* ..... *Y. Tomita, R. Yahalom, K. Kyuma, A. Yariv, and N. S.-K. Kwong* 315
Polarization-Preserving Phase Conjugation and Temporal Reversal of an Arbitrarily-Polarized Pulsed Optical Signal by Means of Time-and-Space Domain Holography ..... *P. M. Saari, R. K. Kaarli, R. V. Sarapuu, and H. R. Sonajalg* 339
Phase Conjugation of Single Photons ..... *N. F. Andreev, V. I. Bespalov, M. A. Dvoretsky, and G. A. Pasmanik* 346
Generalized Phase-Conjugation System Using Partially-Coherent Light ..... *A. Cunha and E. N. Leith* 351

Four-Wave Mixing Interactions

Phase Conjugation of CO_2 Laser Radiation in a Medium with Thermal Nonlinearity ..... *V. I. Bespalov, A. A. Betin, E. A. Zhukov, O. V. Mitropol'sky, and N. Yu. Rusov* 360
Probe Beam Amplification and Phase Conjugation Self-Oscillation in a Thin Kerr Medium ..... *I.-C. Khoo and Y. Zhao* 368
Transient Coherent Degenerate Four-Wave Mixing ..... *J.-T. Chen and Z.-X. Yu* 373
The Influence of Velocity-Changing Collisions on Resonant Degenerate Four-Wave Mixing ..... *W. H. Richardson, L. Maleki, and E. Garmire* 382
Conical Emissions and Phase Conjugation in Atomic Sodium Vapor ..... *J. Pender and L. Hesselink* 395
Nonlinear Complex Susceptibility of Cresyl Violet Solution Measured with a Dynamic Grating Method ..... *N. Wiese, H. J. Eichler, and J. Salk* 403

(Contents Continued on Back Cover)

IEEE JOURNAL OF

QUANTUM ELECTRONICS

MARCH 1989 VOLUME 25 NUMBER 3 (ISSN 0018-9197)

A PUBLICATION OF THE IEEE LASER AND ELECTRO-OPTICS SOCIETY

SPECIAL ISSUE ON NONLINEAR OPTICS AND PHASE CONJUGATION

QUANTUM ELECTRONICS LETTERS

RF-Excited Tunable CO Laser with Opto-Hertzian Frequency Stabilization ..... *G. N. Pearson and D. R. Hall* 245
Improved Coupled-Mode Theory of Anisotropic Optical Waveguides ..... *T. Feng, G. Feng, Y.-Z. Wu, and P.-D. Ye* 249
Electrooptic Diffraction Modulation in ZnO Film on Sapphire ..... *M.-S. Wu, T. Shiosaki, and A. Kawabata* 252

REGULAR PAPERS

Semiconductor Lasers

Efficient Frequency Noise Reduction of GaAlAs Semiconductor Lasers by Optical Feedback from an External High Finesse Resonator ..... *H. Li and H. R. Telle* 257
Optical Polarization Bistability in TM Wave Injected Semiconductor Lasers ..... *Y. Mori, J. Shibata, and T. Kajiwara* 265

Nonlinear Optics in Fibers

Theory of Stimulated Raman Scattering in Optical Fibers in the Pulse Walkoff Regime ..... *D. N. Christodoulides and R. I. Joseph* 273
Noise Characterization of Femtosecond Fiber Raman Soliton Lasers ..... *U. Keller, K. D. Li, M. Rodwell, and D. M. Bloom* 280

Other Papers

Criteria for Optical Bistability in a Lossy Saturating Fabry–Perot ..... *E. Garmire* 289
Matrix Formalism for Dispersive Laser Cavities ..... *O. E. Martínez* 296
Theoretical Investigation of an Integrated All-Optical Controller–Modulator Device Using QCSE in a Multiquantum Well Phototransistor ..... *S. Hong and J. Singh* 301

SPECIAL ISSUE PAPERS

Introduction to the Special Issue ..... *D. M. Pepper* 312

Propagation, Low-Level Signals, and Superresolution

Polarization and Spatial Information Recovery by Modal Dispersal and Phase Conjugation: Properties and Applications *(Invited Paper)* ..... *Y. Tomita, R. Yahalom, K. Kyuma, A. Yariv, and N. S.-K. Kwong* 315
Polarization-Preserving Phase Conjugation and Temporal Reversal of an Arbitrarily-Polarized Pulsed Optical Signal by Means of Time-and-Space Domain Holography ..... *P. M. Saari, R. K. Kaarli, R. V. Sarapuu, and H. R. Sonajalg* 339
Phase Conjugation of Single Photons ..... *N. F. Andreev, V. I. Bespalov, M. A. Dvoretsky, and G. A. Pasmanik* 346
Generalized Phase-Conjugation System Using Partially-Coherent Light ..... *A. Cunha and E. N. Leith* 351

Four-Wave Mixing Interactions

Phase Conjugation of CO_2 Laser Radiation in a Medium with Thermal Nonlinearity ..... *V. I. Bespalov, A. A. Betin, E. A. Zhukov, O. V. Mitropol'sky, and N. Yu. Rusov* 360
Probe Beam Amplification and Phase Conjugation Self-Oscillation in a Thin Kerr Medium ..... *I.-C. Khoo and Y. Zhao* 368
Transient Coherent Degenerate Four-Wave Mixing ..... *J.-T. Chen and Z.-X. Yu* 373
The Influence of Velocity-Changing Collisions on Resonant Degenerate Four-Wave Mixing ..... *W. H. Richardson, L. Maleki, and E. Garmire* 382
Conical Emissions and Phase Conjugation in Atomic Sodium Vapor ..... *J. Pender and L. Hesselink* 395
Nonlinear Complex Susceptibility of Cresyl Violet Solution Measured with a Dynamic Grating Method ..... *N. Wiese, H. J. Eichler, and J. Salk* 403
Optical Phase Conjugation and Nonlinear Optical Bandpass Filter Characteristics in CdSSe Microcrystallite-Doped Glass ..... *J. T. Remillard, H. Wang, M. D. Webb, and D. G. Steel* 408

Stimulated Brillouin Scattering

The Structure of the Stokes Fields Reflected in SBS in a Light Guide ..... *I. Yu. Anikeev, D. A. Glazkov, A. A. Gordeev, I. G. Zubarev, A. B. Mironov, and S. I. Mikhailov* 414

Application of a Phase-Conjugate Brillouin Mirror to Generation of High-Quality Variable-Duration KrF Pulses ..... *N. A. Kurnit and S. J. Thomas* 421

Large Signal Characteristics of Stimulated Brillouin Scattering and Gaussian Beam Phase Conjugation ..... *H. Hsu and S.-S. Bor* 430

Brillouin-Enhanced Four-Wave Mixing (Hypersonic Interactions)

A Review of Brillouin-Enhanced Four-Wave Mixing *(Invited Paper)* ..... *A. M. Scott and K. D. Ridley* 438

Polarization-Decoupled Brillouin-Enhanced Four-Wave Mixing ..... *W. A. Schroeder, M. J. Damzen, and M. H. R. Hutchinson* 460

Hypersonic Phase-Conjugation Mirror for the Reflection of High-Power Nanosecond Pulses ..... *N. G. Basov, D. A. Glazkov, V. F. Efimkov, I. G. Zubarev, S. A. Pastukhov, and V. B. Sobolev* 470

Improved Performance from Noncollinear Pumping in a High-Reflectivity Brillouin-Enhanced Four-Wave Mixing Phase Conjugator ..... *J. R. Ackerman and P. S. Lebow* 479

Two-Beam Coupling, The Photorefractive Effect, and Transient Effects

Two-Wave Mixing in Nonlinear Media *(Invited Paper)* ..... *P. Yeh* 484

Thermal Grating-Mediated Wave Mixing and Beam Amplification in Nematic Liquid Crystal Thin Films ..... *P. Y. Yan and I.-C. Khoo* 520

Vectorial Solution to the Photorefractive Band Transport Model in the Spatial and Temporal Fourier Transformed Domain ..... *P. M. Johansen* 530

Transient Phase Conjugation in Kerr-Media, Photorefractive Media, and Plasmas: A Comparison ..... *G. C. Papen, J. A. Tataronis, and B. E. A. Saleh* 540

Oscillators, Resonators, and Coherent Coupling

Photorefractive Oscillators *(Invited Paper)* ..... *B. Fischer, S. Sternklar, and S. Weiss* 550

Self-Oscillation of a Cavity Using a Phase-Conjugate Amplifier: Study of the Stationary Regime ..... *M. Pinard, R. Horowicz, D. Grandclément, and G. Grynberg* 570

Four-Wave Mixing Oscillation in a Cavity Using Sodium Vapor ..... *D. Grandclément, M. Pinard, and G. Grynberg* 580

Transverse-Mode Structure of a Phase-Conjugate Oscillator Based on Brillouin-Enhanced Four-Wave Mixing ..... *M. D. Skeldon and R. W. Boyd* 588

Optical Phase-Conjugate Feedback Effects on Gain-Guided Diode Laser Characteristics ..... *Y. Champagne, N. McCarthy, and R. Tremblay* 595

Polychromatic Phase Conjugation in Fabry–Perot Etalons ..... *G. Manneberg and M. Kull* 602

Coherent Coupling of CW Laser Oscillators Using Intracavity Four-Wave Mixing ..... *W. P. Brown, C. J. Gaeta, R. C. Lind, and C. R. Giuliano* 607

Optical Computing and Information Processing

Nonlinear Holographic Associative Memories *(Invited Paper)* ..... *Y. Owechko* 619

Optical Novelty Filters *(Invited Paper)* ..... *D. Z. Anderson and J. Feinberg* 635

BOOK REVIEWS

Photovoltaic Power Generation, Proceedings of the Second Contractors' Meeting—R. van Overstraeten and G. Caratti, Eds. ..... *Reviewed by P. Iles* 648

Announcing a Special Issue of the IEEE JOURNAL OF QUANTUM ELECTRONICS on Lasers in Biology and Medicine

A SPECIAL ISSUE devoted to advances in the use of lasers in biology and medicine has been scheduled for March 1990. The role of lasers in biology and medicine, as therapeutic and diagnostic tools as well as lasers in biomedical research, is of great importance. Laser-induced thermal, photochemical, and mechanical tissue effects are currently being used successfully in various medical specialties and explored for future possible therapeutic applications. Moreover, new laser technology including miniaturized laser sources, short-pulse solid-state lasers, and novel optical fiber delivery systems have stimulated investigation of new medical laser applications and further basic research of laser–tissue interaction. New diagnostic techniques such as subnanosecond time-resolved spectroscopy are being used for characterizing biological tissue and measuring optical properties of tissue *in vivo*. Modeling of biological laser interaction such as light propagation in tissue or linear and non-linear energy dissipation in tissue have already led to a deeper understanding of laser-generated effects in biological material and, in turn, initiated new experimental studies. Previous special issues in December 1984 and October 1987 featured some of these applications.

This Special Issue for 1990 will contain both invited and contributed papers. Contributed papers are solicited in the following areas:

- new applications of lasers in biology and medicine
- experimental and theoretical studies of laser–tissue interactions
- applications of laser spectroscopy in medicine and biology
- new laser and optical fiber technology for medical applications.

The deadline for submission of manuscripts is **June 15, 1989.** Original contributions may be submitted in letter format announcing most recent ideas and results or as regular-length papers. Three copies of the manuscript plus original figures, photographs and biographies (*for papers*), accompanied by a complete copyright form, must be submitted. The references for each citation must include the full title and the beginning and ending page numbers. The contributions should be submitted directly to one of the Guest Editors:

Reginald Birngruber
Harvard Medical School
Wellman Laboratories of Photomedicine
Massachusetts General Hospital
Boston, MA 02114

Jeffrey M. Isner
Tufts University School of Medicine
St. Elizabeth's Hospital
736 Cambridge St.
Boston, MA 02135

Announcing a Special Issue of the IEEE JOURNAL OF QUANTUM ELECTRONICS on Ultrafast Phenomena

THE ongoing rapid advances in ultrashort pulse laser science, technology, and related instrumentation have continued to generate a wealth of activities, increasingly encompassing new areas in physical sciences. The IEEE JOURNAL OF QUANTUM ELECTRONICS has played an active role in disseminating news about developments in both ultrashort pulse sources and their use in spectroscopy and engineering applications. Striking progress has occurred in the past two to three years where substantial reduction in the pulsewidth, increases in wavelength tunability and peak power, and many improvements in the measurement technology have now led to the study of a wide range of basic and applied phenomena on a femtosecond timescale. In recognition of these advances, a Special Issue of the IEEE JOURNAL OF QUANTUM ELECTRONICS will be devoted to recent developments of the subject, with emphasis on fundamental science associated with ultrafast phenomena. The issue will include both invited and contributed papers. Contributions will be welcome which involve physics of sources, new methods for generating ultrashort optical pulses, transient spectroscopy of condensed matter including liquids, metals, semiconductors and material microstructures, interaction of intense laser radiation with matter, and solitons and nonlinear pulse propagation.

The deadline for submission is **March 31, 1989.** Publication of the Special Issue is scheduled for December 1989. Additional information for authors is found on the inside back cover of current issues of the IEEE JOURNAL OF QUANTUM ELECTRONICS. Contributions should consist of an original plus two copies of the manuscript and a set of original figures in a form suitable for reproduction. Manuscripts must be accompanied by a completed copyright form, which can be found in any January issue of this JOURNAL. Full reference titles, together with the beginning and ending page numbers for each citation, should be included in the reference list. Contributions should be submitted directly to one of the Guest Editors:

J. G. Fujimoto
Department of Electrical Engineering and Computer Sciences
Massachusetts Institute of Technology
Cambridge, MA 02139
(617) 253-8528

A. V. Nurmikko
Division of Engineering
Brown University
Providence, RI 02912
(401) 863-2869

Quantum Electronics Letters

RF-Excited Tunable CO Laser with Opto-Hertzian Frequency Stabilization

G. N. PEARSON AND D. R. HALL

Abstract—**We describe an RF-excited tunable CO laser, of cavity length 46.6 cm, operating sealed-off with coolant at −5° C. Frequency stabilization has been achieved using the opto-Hertzian effect, which induces a correlation between the laser and the reflected RF powers.**

SEVERAL experimental techniques for the analysis of gases require a tunable infrared radiation source. These include photoacoustic [1], absorption [2], and optogalvanic spectroscopy [3]. The emission wavelengths of the CO laser, operating at temperatures near ambient, encompass the range 5–6 μm, which overlaps the absorption bands of numerous gases such as NO, NO_2, N_2O_4, and C_2H_4. A stable, step-tunable CO laser source is therefore a useful tool for the detection of such gases as atmospheric pollutants. Lasers of this type are also used to pump spin-flip Raman lasers [4] and are needed for measurements of gain in CO amplifiers [5], [6].

The emission spectrum of a CO laser employing a Littrow mounted grating cavity does not always consist of a single vibrational-rotational transition. There is gain on all vibrational transitions for which the vibrational temperature is in excess of the threshold value. This multilevel system of laser transitions results in regions of the spectrum where gain is available on lines whose frequency separation is <0.5 cm^{-1}. For some of these spectral regions the dispersion of the optical resonator may not be sufficient to resolve the lines and this can result in simultaneous oscillation on several lines. There are however, certain regions of the CO laser spectrum where single frequency operation is possible. Single line powers of >2 W have been obtained from a laser 1.9 m in length [7]. The number of single lines available can be increased by varying the operating parameters, but this is always accompanied by a reduction in the laser power. External Fabry–Perot interferometers can be used to produce single frequency emission [8] but these add to the complexity of the laser. An alternative approach is to reduce the cavity length since this causes an increase in the axial mode spacing. We report here results for a tunable CO laser with a gain length of 38.6 cm and a cavity length of only 46.6 cm. This cavity has an axial mode spacing of $\simeq 320$ MHz.

The laser gain region was constructed from a pair of alumina slabs and two aluminum electrodes. These were clamped together to form a square section discharge volume of dimensions 6 × 6 × 386 mm. The discharge structure capacitance was $\simeq 90$ pF and was operated under conditions of near resonance using distributed parallel inductors. Cooling was achieved by flowing methanol through a circuit formed within the ground electrode. RF power at 53 MHz was supplied to the center of the top electrode via an *LC* matching network. The forward and reflected RF power could be monitored using a bidirectional Bird Thruline signal pick-off (4522.002). The optical cavity was formed by a 4 m radius of curvature dielectric coated (R = 99.4 percent) silicon mirror and a Littrow mounted grating with 150 lines/mm, blazed for 5.4 μm. The optics were mounted on a pair of invar bars and were separated from the ends of the discharge by a distance of 4 cm. The silicon mirror was mounted on a piezoelectric transducer which produced an extension of 15 μm for an applied voltage of 150 V. A low voltage device was chosen because of the need for intravacuum operation.

The whole assembly was housed in an aluminum box which served as the vacuum envelope. The grating angle and the mirror alignment could be adjusted, while the laser was running, via vacuum feed-throughs. The laser power was extracted from the cavity using the zeroth order from the grating. We did not employ a coupled mirror to produce a constant exit angle of the beam, hence the beam emerged from the laser box via a rectangular calcium fluoride window whose dimensions were chosen in order to permit operation over the spectral region 5–6 μm.

The laser operated sealed-off at pressures between 20 and 40 torr with an optimum of 33 torr. The coolant temperature was held at −5° C. For these experiments we used a premixed gas of 2.53 percent CO, 3.52 percent Xe, 18 percent N_2, and balance He. 0.04 percent oxygen was added to produce a more stable discharge. We observed >50 discrete transitions within the wavelength range 5.2–5.8 μm. The powers ranged from 10–500 mW. For regions of single frequency output, the maximum power we obtained was 90 mW. The signature of the $P_9(22)$ (5.4138

Manuscript received June 29, 1988; revised October 13, 1988. This work was supported by an S.E.R.C. CASE Award from Laser Applications Ltd.

The authors are with the Department of Physics, Heriot-Watt University, Riccarton, Edinburgh, EH14 4AS Scotland.

IEEE Log Number 8825865.

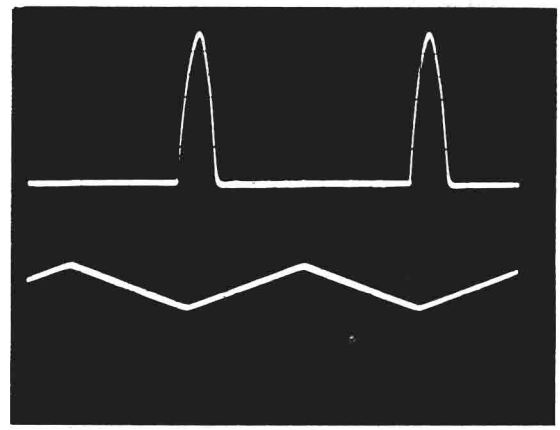

Fig. 1. Signature of the $P_9(22)$ transition. Upper trace is the laser power, lower trace is the bias applied to the piezoelectric tranducer.

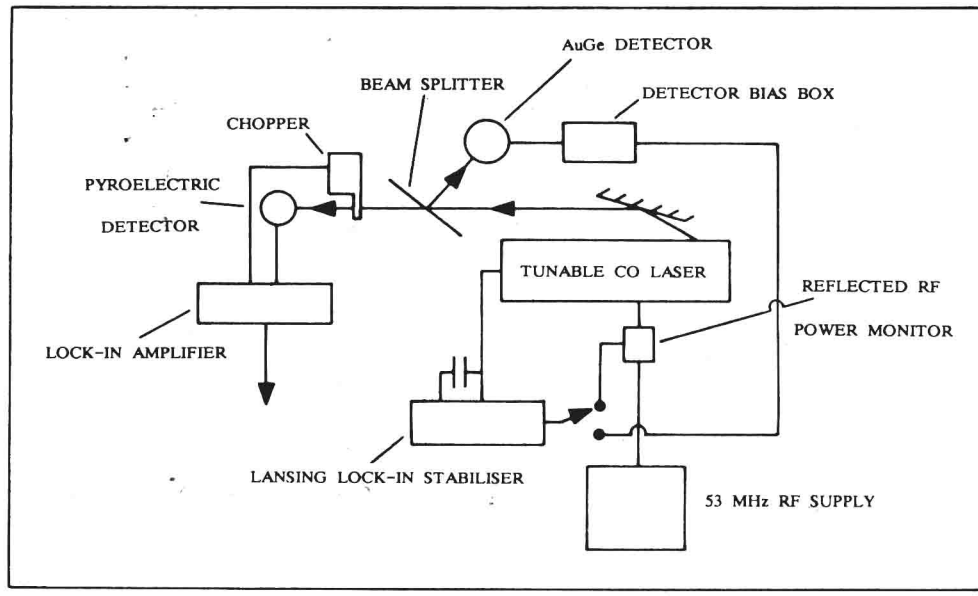

Fig. 2. The photodetector and reflected RF schemes for detecting the laser power modulation.

μm) is shown in Fig. 1. The lower trace shows the voltage ramp applied to the piezoelectric transducer.

To stabilize the laser output we initially used a calcium fluoride beam splitter to couple 5 percent of the output to a liquid nitrogen cooled AuGe detector. A Lansing (model 80.215) lock-in stabilizer was then used to induce a 518 Hz sinusoidal dither on the cavity length. The bias and dither amplitudes were then adjusted, with reference to the stabilizer discriminator signal, to select the optimum point for stabilization in the conventional manner. This technique resulted in satisfactory frequency stabilization. We then investigated the effects of the laser power modulation on the reflected RF power as detected by the Bird signal pick-off. A schematic diagram of the two detection systems is shown in Fig. 2.

The optogalvanic effect is well known for dc-excited CO_2 and CO lasers [9]–[11]. Modulation of the intracavity optical flux results in a modulation of the discharge resistance which can be detected as a modulation in the discharge current. In the case of an RF-discharge-excited laser this resistance modulation produces a modulation of the impedance match between the RF supply and the laser head. The magnitude of the reflected RF power is very sensitive to the impedance match and therefore the laser power modulation can be detected as a modulation in the reflected RF power. This phenomena has been observed and analyzed previously with respect to RF-excited CO_2 waveguide lasers [12]. A 100 percent modulation of the cavity flux present for a laser output power of 100 mW was shown to produced a modulation of the discharge resistance of $\simeq 1$ percent. Attempts to use this system for frequency stabilization were not successful. However, the CO laser described here was very successfully stabilized using this technique of monitoring the reflected RF power signal. Fig. 3 illustrates this effect as exhibited by our laser. The top trace is the filtered reflected RF power signal and the bottom trace is the dither voltage applied to the piezoelectric transducer. Fig. 3 illustrates the maxi-

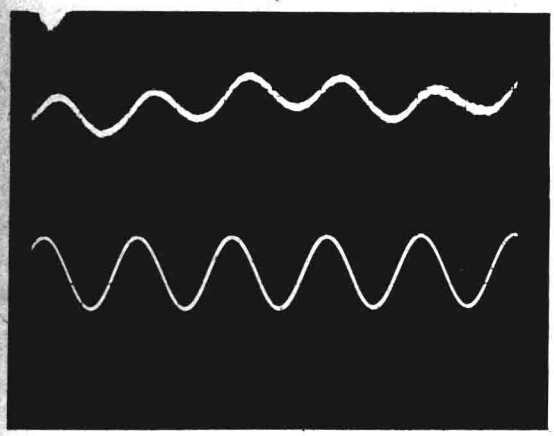

Fig. 3. Opto-Hertzian signal. Top trace is the reflected RF power signal (2 mV peak-to-peak), bottom trace is the 518 Hz dither applied to the piezoelectric transducer (1 V peak-to-peak).

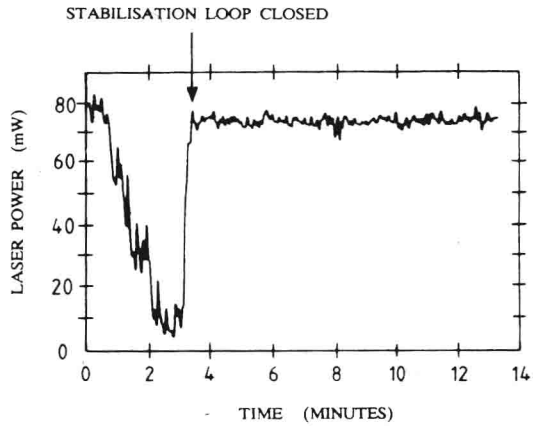

Fig. 4. Laser power versus time with opto-Hertzian closed loop stabilization on and off.

mum signal which was obtained when the bias and modulation voltages were set so as to produce a cavity tuning over the high gradient region of the transition signature. For the case of Fig. 3, the 1 V peak-to-peak transducer voltage produced a cavity tuning of $\simeq$ 12 MHz which corresponded to a $\simeq 20$ percent modulation of the laser power. Under optimum conditions, the maximum frequency deviation of the stabilized cavity was $\simeq 5$ MHz.

The relative sensitivity of this stabilization scheme, for different grating angles, was dependent upon the respective signature profiles and cavity fluxes. The $P_9(22)$ line was the highest power single transition which lased and consequently this line exhibited the maximum stability. For regions of the tuning range where the resultant signature consisted of the convolution of the signatures of several transitions, the stability of the laser was impaired due to the reduced sensitivity of the laser power on the cavity tuning.

To observe this signal the reflected RF power must be nonzero. The laser operated with 50 W of RF input and 3 W reflected. This degree of mismatch was found to be quite sufficient to produce a detectable signal. Using this so called *opto-Hertzian* effect we successfully stabilized the laser to the center of the chosen line. This is shown in Fig. 4 for the $P_9(22)$ line. Here we show the laser power variation with time for stabilized and unstabilized laser cavity. We found that the amplitudes of modulation required to produce stabilization lock were very similar for both the optically detected and reflected RF power detected cases. By adjusting the grating, bias, and modulation settings we could produce a nonsinusoidal modulation of the laser amplitude. Fig. 5 shows these more complex periodic fluxations are also accurately induced in the reflected RF signal.

When the cavity was actively stabilized, this laser exhibited good power stability over periods of approximately 10 min (see Fig. 4). Over longer periods of time than this ($\simeq 30$ min), the laser power gradually decreased. This was attributed to drifts in the alignment of the resonator due to inadequate thermal and mechanical isolation

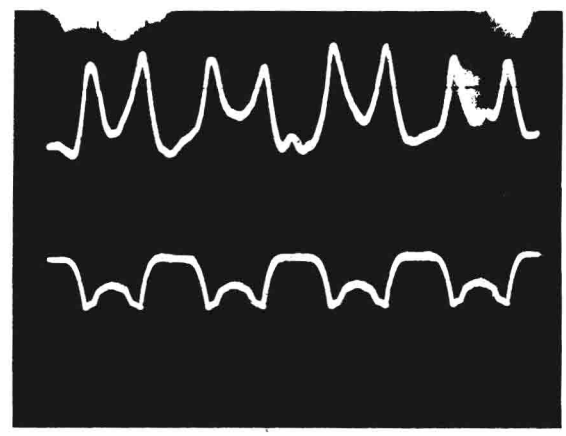

Fig. 5. Opto-Hertzian effect for nonsinusoidal laser power periodicity. Top trace is the reflected RF power, bottom trace is the laser power.

since the laser power could be re-established by adjusting the cavity optics. Daily changing of the gas charge was necessary in order to maintain optimum performance.

To conclude, we have demonstrated both a novel tunable CO laser design and a novel technique with which to produce frequency stabilization. This opto-Hertzian detection is quite sensitive enough to produce an excellent signal correlated to the modulation of the laser power. This stabilization scheme is similar to photoacoustic [13] and optogalvanic stabilization in that it does not require the useful laser output to be monitored in any way.

ACKNOWLEDGMENT

The authors wish to thank Dr. K. Abramski and Dr. P. E. Jackson for informative discussions and S. Haughey for his expert technical assistance.

REFERENCES

[1] S. Bernegger and M. N. Sigrist, "Longitudinal resonant spectrophone for CO laser photoacoustic spectroscopy," *Appl. Phys. B.*, vol. 44, pp. 125–132, 1987.

[2] R. T. Menzies, "Use of CO and CO_2 lasers to detect pollutants in the atmosphere," *Appl. Opt.*, vol. 10, pp. 1532–1538, 1971.

[3] C. Stanciulescu, R. C. Bobulescu, A. Surmeian, D. Popescu, and I. I. Popescu, "Hertzian and optical impedance spectroscopy," *Rev. Rouman. Phys.*, vol. 25, no. 8, pp. 915–926, Bucharest, Romania, 1980.

[4] C. K. N. Patel, "Stimulated second Stokes spin-flip Raman scattering in InSb," *Appl. Phys. Lett.*, vol. 18, pp. 274–276, 1971.

[5] P. Brechignac, J. P. Martin, and G. Taieb, "Small signal gain and vibrational distribution in CO," *IEEE J. Quantum Electron.*, vol. QE-10, pp. 797–802, 1974.

[6] M. L. Bhaumik, W. B. Lacina, and M. M. Mann, "Characteristics of a CO laser," *IEEE J. Quantum Electron.*, vol. QE-8, pp. 150–160, 1972.

[7] M. J. Colles, R. B. Dennis, J. S. Webb, J. W. Smith, and R. L. Allwood, "Near room temperature cw CO laser with a high single frequency output," *Opt., Laser Technol.*, pp. 73–74, April. 1975.

[8] R. B. Dennis, H. A. Mackenzie, G. McClelland, and F. H. Hamza, "Investigation of the specral content of a cw CO laser output using a high resolution scanning Fabry-Perot interferometer," *Opt., Laser Technol.*, pp. 221–226, Oct. 1976.

[9] A. L. S. Smith and D. Moffat, "Opto-Galvanic stabilized CO_2 laser," *Opt. Commun.*, vol. 30, pp. 213–218, 1979.

[10] M. C. Skolnick, "Use of plasma tube impedance variations to frequency stabilize a CO_2 laser," *IEEE J. Quantum Electron.*, vol. QE-6, pp. 139–140, 1970.

[11] K. M. Abramski, J. van Spijker, and W. J. Witteman, "On the opto-voltaic measurements in CO and CO_2 lasers," *Appl. Phys. B.*, vol. 36, pp. 149–153, 1985.

[12] P. E. Jackson, K. M. Abramski, and D. R. Hall, "Automatic impedance matching and opto-Hertzian effect in RF excited CO_2 waveguide lasers," *Appl. Phys. B*, vol. 47, pp. 149–157, 1988.

[13] M. I. Abu-Taha and D. C. Laine, "Frequency stabilization of a CO_2 gas laser by intra-cavity optoacoustic absorption," in *Proc. 8th Nat. Quantum Electron. Conf.*, St. Andrews, U.K., Sept. 21–25, 1987, paper 18P.

Improved Coupled-Mode Theory of Anisotropic Optical Waveguides

FENG TIAN, FENG GAO, WU YIZUN, AND YE PEIDA, FELLOW, IEEE

Abstract—**The improved coupled-mode theory [1] is extended to include anisotropic optical waveguides. A coupled-mode equation for anisotropic waveguide systems of arbitrary cross section and general dielectric distribution is derived in a much simpler way. New numerical results are presented to compare the exact calculations with the Hardy *et al.* formulations [9] and with ours in the case of anisotropic waveguides, which shows that the same accuracy can be obtained from our formulations and [9].**

I. Introduction

THE coupled-mode theory has played a very important role in the fields of integrated optics and semiconductor laser arrays since the 1970's. Great improvements of the theory have been made recently [1]–[6], which gives more accurate results and makes the theory applicable to the analysis of moderately strong coupling in optical waveguide systems.

The major improvement of the theory is that it considers the interaction of the individual waveguide modes to be so important that the overlap integrals c_{pq} defined in [1] cannot be neglected in the derivation of the coupled-mode equation. Nevertheless, the previous coupled-mode theories [7], [8] did not take into account the overlap integrals, so their results are applicable only in special cases of near identical waveguides in weak coupling situations. In contrast, the improved coupled-mode formulations can be applied to any guided modes (TE, TM, or hybrid) in waveguides of arbitrary cross section, dissimilar index, and nonidentical shape.

However, most integrated optical devices are made of anisotropic materials in practice. The permittivities of these waveguide systems are characterized by a dielectric tensor:

$$\overleftrightarrow{\epsilon} = \begin{pmatrix} \epsilon_{xx} & \epsilon_{xy} & \epsilon_{xz} \\ \epsilon_{yx} & \epsilon_{yy} & \epsilon_{yz} \\ \epsilon_{zx} & \epsilon_{zy} & \epsilon_{zz} \end{pmatrix}. \tag{1}$$

Generally, $\overleftrightarrow{\epsilon}$ is complex when there exists loss or gain in waveguide systems. For the lossless case, it is Hermitian, and for isotropic media, it degenerates to a scalar. Some extension of the improved coupled-mode theory has been made to anisotropic media in multiwaveguide systems for some special cases ($\epsilon_{xz} = \epsilon_{yz} = \epsilon_{zx} = \epsilon_{zy} = 0$) [9], and significant work [10] was reported after the original manuscript of this paper was submitted.

In this paper, further improvement of the coupled-mode theory is made to extend the application of the theory to general anisotropic optical waveguide systems with arbitrary dielectric tensors. Starting from Maxwell's curl equations, we derive the coupled-mode equation for anisotropic waveguide systems in a way much simpler than those derivations published previously, including [10]. For simplicity, we neglect radiation modes in the derivation, and ignore the very small discrepancy caused by our expression for the longitudinal component of the electric field of the entire system because of the weakly guiding condition. However, specific examples of two coupled anisotropic slab waveguides show that our results have the same accuracy as the formulations of Hardy *et al.* [9].

In Section II, we present the derivation of the coupled-mode equation for anisotropic waveguide systems. Section III shows specific examples of two coupled anisotropic slab waveguides and comparisons of the exact calculations and those of the Hardy *et al.* formulations are presented. Finally, we give conclusions in Section IV.

II. Formulation

The formulation developed in this section is based on the two curl equations of Maxwell, i.e.,

$$\nabla \times \boldsymbol{E} = i\omega\mu\boldsymbol{H} \tag{2}$$

$$\nabla \times \boldsymbol{H} = -i\omega\overleftrightarrow{\epsilon} \cdot \boldsymbol{E} \tag{3}$$

where we have used $\exp(-i\omega t)$ to describe the time dependence of the fields.

A system of anisotropic N waveguides which is invariant in z is characterized by a dielectric tensor $\overleftrightarrow{\epsilon}(x, y)$. The guides are in general not identical, and their relative locations are arbitrary. Each isolated guide, numbered $n = 1, 2, \cdots, N$, has its own dielectric distribution $\overleftrightarrow{\epsilon}_n(x, y)$, and the other waveguides form a perturbation to it, which is defined by

$$\Delta\overleftrightarrow{\epsilon}_n(x, y) = \overleftrightarrow{\epsilon}(x, y) - \overleftrightarrow{\epsilon}_n(x, y). \tag{4}$$

We assume that each individual waveguide supports only a single guided mode [$\boldsymbol{E}_n(x, y) \exp(i\beta_n z)$, $\boldsymbol{H}_n(x, y) \exp(i\beta_n z)$] with a propagation constant β_n, $n = 1, 2, \cdots, N$. The extension to a multiple-mode waveguide is straightforward by including a summation over all the guided modes in each waveguide. Therefore, the total

Manuscript received September 28, 1987; revised September 14, 1988.

T. Feng, Y.-Z. Wu, and P.-D. Ye are with the Optical Communication Laboratory, Beijing University of Posts Telecommunications, Beijing, People's Republic of China.

G. Feng is with the Microwave Laboratory, The Department of Radio and Electronics, Tsinghua University, Beijing, People's Republic of China.

IEEE Log Number 8825870.

electromagnetic field which propagates in the $+z$-direction along an anisotropic waveguide system can approximately be described as

$$\boldsymbol{E}(x, y, z) = \sum_{n=1}^{N} c_n(z)\, \boldsymbol{E}_n(x, y) \tag{5}$$

$$\boldsymbol{H}(x, y, z) = \sum_{n=1}^{N} c_n(z)\, \boldsymbol{H}_n(x, y). \tag{6}$$

Substituting (4)–(6) into (2) and (3) and noticing that

$$\nabla \times [\boldsymbol{E}_n \exp(i\beta_n z)] = i\omega\mu \boldsymbol{H}_n \exp(i\beta_n z) \tag{7}$$

$$\nabla \times [\boldsymbol{H}_n \exp(i\beta_n z)] = -i\omega \overleftrightarrow{\epsilon}_n \cdot \boldsymbol{E}_n \exp(i\beta_n z), \tag{8}$$

we obtain

$$\sum_{n=1}^{N} \nabla c_n \times \boldsymbol{E}_n = \sum_{n=1}^{N} i\beta_n \hat{z} \times \boldsymbol{E}_n c_n \tag{9}$$

$$\sum_{n=1}^{N} \nabla c_n \times \boldsymbol{H}_n = -i\omega \sum_{n=1}^{N} c_n \Delta\overleftrightarrow{\epsilon}_n \cdot \boldsymbol{E}_n + \sum_{n=1}^{N} i\beta_n \hat{z} \times \boldsymbol{H}_n c_n \tag{10}$$

where $\nabla c_n = dc_n/dz\, \hat{z}$.

We take the scalar product of (9) with $\boldsymbol{H}_m$ and of (10) with $-\boldsymbol{E}_m$, then add the two equations, and integrate over the infinite cross section. The result of this procedure is

$$\boldsymbol{AC}' = i\boldsymbol{ABC} + i\boldsymbol{KC} \tag{11}$$

where $\boldsymbol{C}'$ denotes $d\boldsymbol{C}/dz$, $\boldsymbol{C} = \mathrm{col}[c_1, c_2, \cdots, c_N]$, and $\boldsymbol{B} = \mathrm{diag}[\beta_1, \beta_2, \cdots, \beta_N]$. The matrix $\boldsymbol{A}$ has elements

$$a_{mn} = \iint \hat{z} \cdot (\boldsymbol{E}_m \times \boldsymbol{H}_n + \boldsymbol{E}_n \times \boldsymbol{H}_m)\, dx\, dy \qquad m, n = 1, 2, \cdots, N, \tag{12}$$

and the matrix $\boldsymbol{K}$ is given by

$$k_{mn} = \omega \iint \boldsymbol{E}_m \cdot \Delta\overleftrightarrow{\epsilon}_n \cdot \boldsymbol{E}_n\, dx\, dy \qquad m, n = 1, 2, \cdots, N. \tag{13}$$

Comparing (11)–(13) with the formulations given by Streifer *et al.* [4], [9], Chuang [5], and Haus *et al.* [6], we can see that they are exactly the same in the special case of isotropic waveguides, except for a little difference in the expression of k_{mn}. In the next section, examples will show that the difference is so small that it can be neglected in practice. It is noticeable that even in the complicated anisotropic situation our derivation is the simplest, and it is the easiest to understand among all derivations of the improved coupled-mode theory.

III. Examples and Discussions

To illustrate the fact that our theory has the same accuracy as that of Hardy *et al.*, we calculate propagation constants for TE and TM modes of Ti-diffused $LiNbO_3$ waveguides, which are used most in practice. Considering two anisotropic slab waveguides as shown in Fig. 1, the thicknesses of the guides are D_1 and D_3, respectively, and the edge-to-edge separation is D_2. The uniaxial axis is assumed to be in the y-direction for both guiding and substrate regions (the principal dielectric axis system is represented by $[a, b, c]$ in Fig. 1). The dielectric distribution of the system is as follows:

$$\overleftrightarrow{\epsilon}_0 = \epsilon_0 \begin{pmatrix} n_{0s}^2 & 0 & 0 \\ 0 & n_{es}^2 & 0 \\ 0 & 0 & n_{0s}^2 \end{pmatrix} \tag{14}$$

$$\overleftrightarrow{\epsilon}_1 = \epsilon_0 \begin{pmatrix} n_{0g}^2 & 0 & 0 \\ 0 & n_{eg}^2 & 0 \\ 0 & 0 & n_{0g}^2 \end{pmatrix}, \tag{15}$$

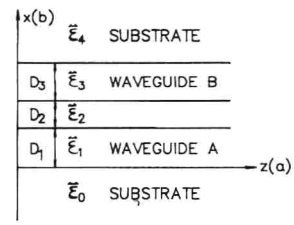

Fig. 1. Dielectric distribution of the anisotropic slab waveguide system under consideration.

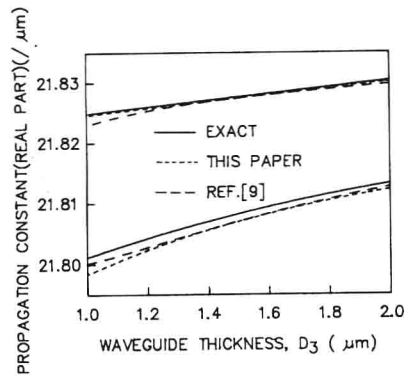

(a)

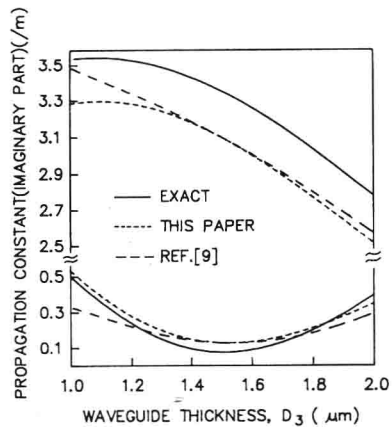

(b)

Fig. 2. Propagation constants of TE modes versus waveguide thickness D_3.

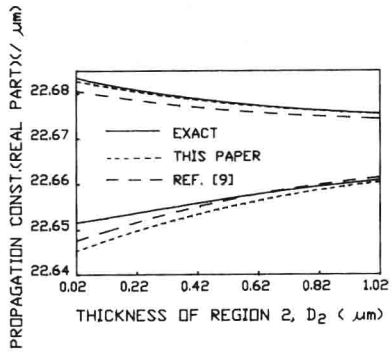

(a)

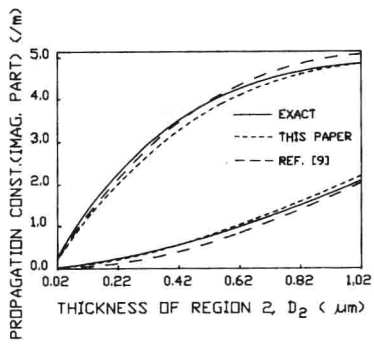

(b)

Fig. 3. Propagation constants of TM modes versus D_2, thickness of region 2.

and Re $(\overleftrightarrow{\epsilon_2}) = \overleftrightarrow{\epsilon_4} = \overleftrightarrow{\epsilon_0}$, $\overleftrightarrow{\epsilon_3} = \overleftrightarrow{\epsilon_1}$, where $n_{0s} = 2.281$, $n_{es} = 2.195$, $n_{0g} = 2.286$, $n_{eg} = 2.2$, and an additional loss exists between the two guides such that Im $(\overleftrightarrow{\epsilon_2})/\epsilon_0 = 1.299 \times 10^{-5}\,\overleftrightarrow{I}$, $\overleftrightarrow{I}$ is the unit tensor. We choose the index variation to be along the x-direction, and therefore, the electric field has only the y-component for TE mode and the x- and z-components for TM mode. The wavelength is $\lambda = 0.6328$ μm.

In Fig. 2, we show the real and imaginary parts of the propagation constants under TE mode coupling. We fix $D_1 = 1.5$ μm and $D_2 = 0.4$ μm and vary D_3, the thickness of waveguide B, between 1 and 2 μm. The numerical results using an exact root-searching approach are shown as solid lines. The dashed curves were determined from [9] and our formulations. Even though the z-component is zero for TE mode, there is a little difference between [9] and our results because of the different expression on coupling coefficients k_{mn}.

In the case of TM modes, we choose another slab waveguide example with $D_1 = 1.5$ μm, $D_3 = 1$ μm, and D_2 changed from 0.02 to 1.02 μm. The propagation constants under this situation are plotted in Fig. 3. It is clear that the difference between [9] and our results is very small. Moreover, it seems that the improved coupled-mode theory is still quite correct when moderately strong coupling occurs under the condition where D_2 is about 0.1 μm.

IV. Conclusions

The improved coupled-mode theory is developed to include anisotropic optical waveguide systems of arbitrary cross section and general dielectric distribution in this paper. We believe that this extension is important because most integrated optical devices are made of anisotropic materials in practice. Even though we handled a more complicated problem of anisotropic media, we present a much simpler derivation of the coupled-mode formulation for anisotropic waveguide systems. Numerical results comparing the exact calculations to those of the method of Hardy *et al.* and ours show that the same accuracy can be obtained not only for TE, but also for TM mode coupling in the case of anisotropic waveguides, and the improved coupled-mode theory is applicable to the situation when moderately strong coupling occurs under the condition where the edge-to-edge separation of two coupled guides D_2 is about 0.1 μm. In the more complex cases, permittivity tensors have nonzero off-diagonal elements caused by applied voltages which change with time and space. It is convenient first to find all modes of the entire multiwaveguide system without the applied voltage, based on our work here, and then to get the analytic solution of the given system using the improved coupled-mode theory for anisotropic waveguide modulators [11].

Acknowledgment

The authors thank Dr. Z. Zheng, Dr. Z. Xiaopin, H. Rongqing, and L. Qiang for helpful discussions.

References

[1] A. Hardy and W. Streifer, "Coupled mode theory of parallel waveguides," *J. Lightwave Technol.*, vol. LT-3, pp. 1135–1146, 1985.
[2] ——, "Coupled modes of multiwaveguide systems and phased arrays," *J. Lightwave Technol.*, vol. LT-4, pp. 90–99, 1986.
[3] ——, "Coupled mode solutions of multiwaveguide systems," *IEEE J. Quantum Electron.*, vol. QE-22, pp. 528–534, 1986.
[4] W. Streifer, M. Osinski, and A. Hardy, "Reformulation of the coupled-mode theory of multiwaveguide systems," *J. Lightwave Technol.*, vol. LT-5, pp. 1–4, 1987.
[5] S. L. Chuang, "A coupled mode formulation by reciprocity and a variational principle," *J. Lightwave Technol.*, vol. LT-5, pp. 5–15, 1987.
[6] H. A. Haus, W. P. Huang, S.Kawakami, and N. A. Whitaker, "Coupled-mode theory of optical waveguides," *J. Lightwave Technol.*, vol. LT-5, pp. 16–23, 1987.
[7] H. F. Taylor and A. Yariv, "Guided wave optics," *Proc. IEEE*, vol. 62, pp. 1044–1060, 1974.
[8] D. Marcuse, *Light Transmission Optics*. New York: Van Nostrand, 1972.
[9] A. Hardy, W. Streifer, and M. Osinski, "Coupled-mode equations for multimode waveguide systems in isotropic or anisotropic media," *Opt. Lett.*, vol. 11, pp. 742–744, 1986.
[10] L. Tsang and S. L. Chuang, "Improved coupled-mode theory for reciprocal anisotropic waveguides," *J. Lightwave Technol.*, vol. LT-6, pp. 304–311, 1988.
[11] T. Feng, Y.-Z. Wu, and P.-D. Ye, "Improved coupled-mode theory for anisotropic waveguide modulators," *IEEE J. Quantum Electron.*, vol. QE-24, pp. 531–536, 1988.

Electrooptic Diffraction Modulation in ZnO Film on Sapphire

MU-SHIANG WU, TADASHI SHIOSAKI, AND AKIRA KAWABATA

Abstract—**An electrooptic Bragg diffraction modulator with high diffraction efficiency has been obtained using a low-loss epitaxial ZnO optical waveguide on a sapphire substrate. An interdigital electrode with a spatial period of 20 μm and an aperture of 3 mm was fabricated directly on the film surface using a photolithographic technique. For the TE_0 mode at 6328 Å, a maximum diffraction efficiency of 98 percent has been obtained from dc to 100 kHz with an applied voltage of about 31 V. The unclamped electrooptic coefficient r_{33} is estimated to be 5.8×10^{-12} m/V, which is much larger than the clamped value of 2.6×10^{-12} m/V listed in the literature.**

I. Introduction

ZnO thin film is one of the important materials for surface acoustic wave (SAW) transducers [1]–[4], bulk acoustic wave transducers [5], [6], acoustooptic devices [7], [8], electrooptic devices [9], [10], and guided optical wave devices [11]–[15] due to its large piezoelectric [16], sizeable elastooptic [17], electrooptic [18], and nonlinear optic coefficients [19], in addition to its high transparency and fairly large refractive indexes over the infrared–visible range. Since optical scattering loss must be low in waveguides for applications, continued efforts have been made to get low-loss ZnO optical waveguides [20].

The electrooptic grating waveguide modulator has the advantage [9] of spatially separating the diffracted beam from the undiffracted beam and thus does not require a separate analyzer or strict control of the waveguide propagation characteristics, as is required by the polarization and cutoff types of waveguide modulators [21], [22]. A number of these modulators can also be incorporated in a single waveguide so that the output of one modulator can be used as the input to the next modulator, and thus it becomes possible to perform a variety of logic and switching functions monolithically. The speed of the electrooptic modulators may also be faster than that of the acoustooptic modulator.

In the present letter, we report an electrooptic Bragg diffraction modulator with high efficiency using an epitaxial ZnO optical waveguide with an optical loss of about 0.5 dB · cm^{-1} on a sapphire substrate. An interdigital electrode with a spatial period of 20 μm and an aperture of 3 mm was fabricated directly on the ZnO film surface by the conventional photolithographic technique without any buffer layer. A diffraction efficiency measurement for the TE_0 mode at 6328 Å was made for different samples with different thicknesses using a dc power supply or an LF oscillator with a frequency from 10 Hz to 100 kHz as the input source for the interdigital electrode. The results are independent of the frequency in the range from dc to 100 kHz. The unclamped electrooptic coefficient r_{33} of ZnO is estimated to be 5.8×10^{-12} m/V, which is much larger than the clamped value of 2.6×10^{-12} m/V listed in the literature [23].

Manuscript received May 5, 1988.

M.-S. Wu is with the Tatung Institute of Technology, Taipei, Taiwan, Republic of China.

T. Shiosaki and A. Kawabata are with the Department of Electronics, Faculty of Engineering, Kyoto University, Kyoto 606, Japan.

IEEE Log Number 8825872.

II. Theory

Fig. 1 shows a schematic diagram of the electrooptic grating waveguide modulator. The c axis of the ZnO is in the plane of the waveguide. When an electric field is applied to the interdigital electrode, the index of refraction is changed, is linearly proportional to the field, and depends on the crystal orientation and light polarization direction.

ZnO has 6 mm symmetry and two important nonvanishing r_{13} and r_{33} electrooptic coefficients. The equation of the index ellipsoid in the presence of an electric field is

$$(1/n_o^2 + r_{13}E_z)X^2 + (1/n_o^2 + r_{13}E_z)Y^2 + (1/n_e^2 + r_{33}E_z)Z^2 = 1 \quad (1)$$

where E_z is the Z component of the applied electric field and n_o and n_e are ordinary and extraordinary refractive indexes, respectively.

Since no mixed terms appear in (1), the principal axes of the new ellipsoid remain unchanged. The lengths of the new semiaxes are

$$n_x = n_o - (1/2)n_o^3 r_{13}E_z \quad (2a)$$

$$n_y = n_o - (1/2)n_o^3 r_{13}E_z \quad (2b)$$

$$n_z = n_e - (1/2)n_e^3 r_{33}E_z. \quad (2c)$$

For the geometry shown in Fig. 1, TE waveguide modes traveling in the y-direction have z-polarization, while TM waveguide modes traveling in the y-direction have x-polarization. The changes in index of refraction corresponding to TE and TM waveguide modes are Δn_z and Δn_x, respectively, where Δn_z and Δn_x are

$$\Delta n_z = -(1/2)n_e^3 r_{33}E_z \quad (\text{TE}) \quad (3a)$$

$$\Delta n_x = -(1/2)n_o^3 r_{13}E_z \quad (\text{TM}). \quad (3b)$$

A periodic electric field set up by an interdigital electrode structure as shown in Fig. 2 gives rise to the peri-

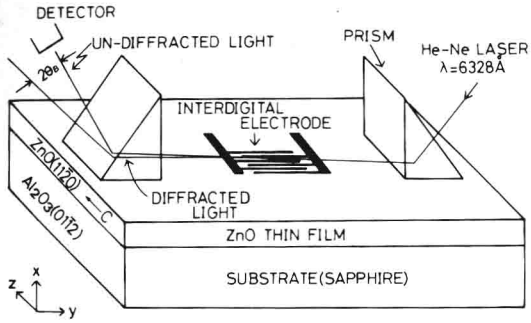

Fig. 1. Schematic diagram of the electrooptic grating waveguide modulator.

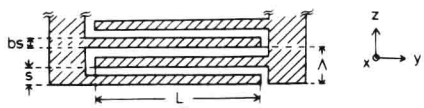

Fig. 2. Configuration of the interdigital electrode.

odic variation of the index of refraction. Parallel metal strips, each of width bs, are situated with distance s between the centers of the strips. The strips are alternately connected to two electrical terminals, giving an electric field of a period of $2s$ ($=\Lambda$) along the z axis. The electrode aperture is L. This electrically controlled phase grating in the path of the propagating beam causes a change in the direction and intensity of the light beam.

The criterion index $Q = 2\pi\lambda L/n\Lambda^2$, where n is the refractive index and λ is the optical wavelength, describes the nature of the diffraction [24]. Bragg diffraction occurs most efficiently when $Q > 10$. When the Bragg condition is satisfied, the optical guided waves are diffracted. The diffracted angle from the direction of the undiffracted beam is $2\theta_B$ where θ_B is the external Bragg angle given by $\theta_B = \sin^{-1}(\lambda/2\Lambda)$ [10]. The diffraction efficiency of Bragg diffraction is [25]

$$I_d/I_i = \sin^2(1/2kL\Delta n) \tag{4}$$

where $k = 2\pi/\lambda$, Δn is the change in refractive index corresponding to TE or TM waveguide mode, and I_i and I_d are the powers of the incident and diffracted beams, respectively.

The electric field in the z-direction in the film is given by [26]

$$E_z = \sum_{n=0}^{\infty} A_{2n+1} \cos\left[(2n+1)\pi z/s\right] \cdot \exp\left[(2n+1)\pi x/s\right] \tag{5}$$

where

$$A_{2n+1} = \pi(V/s)\left[P_n(2k^2-1)/K'(k)\right],$$
$$k = \cos(\pi/2)(1-b),$$

P_n is the Legendre polynomial of the first kind, V is the applied voltage, and $K'(k)$ is the complete elliptic integral of the first kind with the complementary modulus $K' = (1-k^2)^{1/2}$. In an electrode structure constructed so that only the fundamental Fourier component is instrumental in the Bragg diffraction, we can neglect all higher harmonic terms to get [27]

$$E_z = \pi(V/s)\left(1/K'(k)\right)\cos(\pi z/s)\exp(\pi x/s). \tag{6}$$

For the TE_0 mode at 6328 Å, we can obtain an expression for the applied voltage V_f required for 100 percent diffraction from (3), (4), and (6):

$$V_f = s\lambda K'(k)/\left[\pi \exp(\pi x/s) Ln_e^3 r_{33}\right]. \tag{7}$$

Since the distribution of the optical field of the TE_0 mode is roughly symmetrical about the center of the waveguide film, a reasonable estimate might be considered to be obtained by using the value of E_z at the waveguide center, i.e., $x = t/2$ where t is the thickness of the film.

The overall performance of a modulator is usually expressed in terms of a factor PPW, which is equal to the power required per unit bandwidth at 100 percent modulation:

$$\text{PPW} = P/\Delta f = (Vf^2/2R)/(1/\pi RC) = (\pi/2)V_f^2 C \tag{8}$$

where C is the capacitance of the interdigital electrode and R is the resistance. The capacitance C is given by [26]

$$C = \left[\epsilon_0 + (\epsilon_{11}\epsilon_{33})^{1/2}\right]\left[K(k)/K'(k)\right]NL \tag{9}$$

where $K(k)$ is the complete elliptic integral of the first kind with modulus k, N is the number of electrode pairs, and ϵ is the dielectric permittivity. The expression of PPW can be obtained from (7)–(9):

$$\text{PPW} = (1/2\pi)\left[\epsilon_0 + (\epsilon_{11}\epsilon_{33})^{1/2}\right]K(k)\,K'(k)\,(N/L) \times \left[s\lambda/(\exp(\pi t/2s)Ln_e^3 r_{33})\right]^2. \tag{10}$$

III. Results and Discussion

A. Film Fabrication

The RF planar magnetron sputtering system described in [28] was used for the present experiments. A ZnO ceramic, 100 mm in diameter, was used as a sputtering target. A polished wafer of sapphire with $(01\bar{1}2)$ orientation was positioned parallel to the targets.

It is known [29], [30] that the quality of the sputtered films is usually better if the sputtering rate is lower. With this in mind, we modified the sputtering conditions in [28]. We increased the target–substrate spacing from 37 to 47 mm, increased the substrate temperature from 260 to 390°C, and decreased the RF input power from 100 to 50 W. In all the experiments, premixed Ar (50 percent) + O_2 (50 percent) gas was used, and the gas pressure was kept constant at 1×10^{-2} torr. Details of the growth and characterization of ZnO films on sapphire were described elsewhere [20].

Fig. 3 shows the laser light streak in a ZnO thin film. The guided light propagates from the left-hand to the right-hand side, and the length of the observed streak is

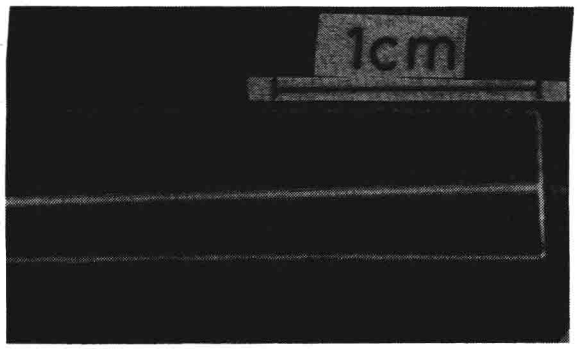

Fig. 3. Photograph of a streak of guided light excited in a ZnO film.

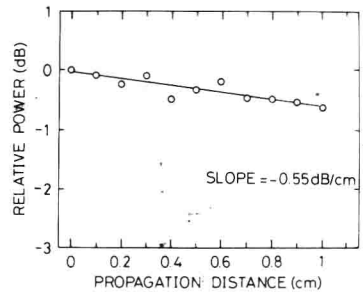

Fig. 4. Optical intensity versus propagation distance for the TE_0 mode of the ZnO film on sapphire.

about 20 mm. Fig. 4 shows the result of the optical loss measurement of a ZnO film on sapphire using the same technique as Channin *et al.* [31]. The optical attenuation for the TE_0 mode of the 6328 Å He–Ne laser light is 0.55 dB · cm^{-1}. To our knowledge, this is the lowest loss that has been reported for an as-grown sputtered ZnO film.

B. Electrooptic Bragg Diffraction Modulation Measurements

Fig. 5 shows the schematic diagram of the electrooptic diffraction modulator measurements. An interdigital electrode of 1000 Å thick Al was fabricated directly onto the ZnO waveguide surface using a photoresist lift-off technique. Fig. 6 is a photograph of a portion of an interdigital electrode used in our experiments. We can see b is approximately $1/2$ as designed. The electrode parameters are given in Table I. At 6328 Å, we find $Q = 15$, indicating that the diffraction in this experiment is strongly governed by Bragg diffraction.

As the interdigital electrode is deposited directly onto the waveguide, the mode characteristics of the waves under the electrode strip and the updated surface are different. Consequently, even with no voltage applied to the modulator, the interdigital electrodes would act as a grating and cause the beam to diffract, and its diffraction angle is expected to be twice the diffraction angle due to the applied electric field.

Two kinds of diffraction efficiencies η_A and η_B are usually used in the experiments. η_A is the fractional decrease in the output from the undiffracted optical beam, and η_B is the ratio of the output of the diffracted optical beam to

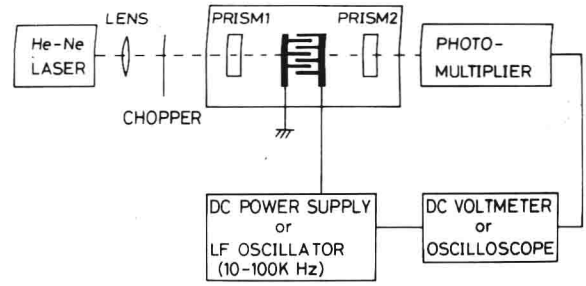

Fig. 5. Schematic diagram of the Bragg diffraction efficiency measurements of the electrooptic diffraction modulators.

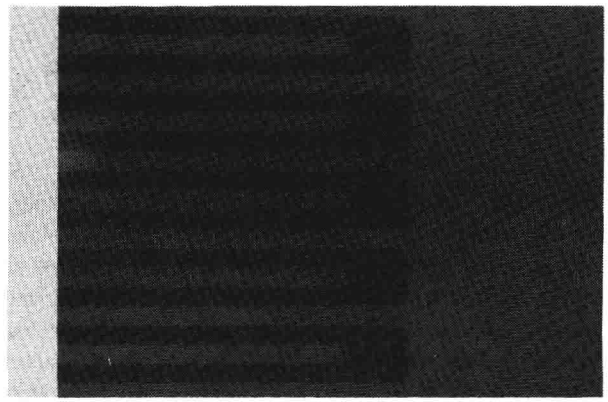

Fig. 6. Photograph of a portion of the interdigital electrode.

TABLE I
PARAMETERS OF THE INTERDIGITAL ELECTRODE

Periodicity of electric field	Λ	20μm
Half periodicity	s	10μm
Electrode width	bs	5μm
Electrode aperture	L	3mm
Electrode finger pairs	N	32
Criterion index	Q	15

that of the undiffracted optical beam. η_A and η_B are equal to I/I_i and I'/I_i, respectively, as shown in Fig. 7.

The results of η_B are deceiving in that the measured diffracted power results from depletion of both the undiffracted beam and the beam caused by the metal grating itself [32]. In some experiments, it can be observed that the diffracted power may actually exceed that of the undiffracted beam. So η_A is more reliable and is used in our measurements.

We measure the diffraction efficiency after aligning the system to give maximum readings when the detector is at the position of the diffracted beam. We use a dc power supply and an LF oscillator with a frequency from 10 Hz to 100 kHz as the input source for the interdigital electrode.

Fig. 8 is a photograph showing a typical oscilloscope display taken under the diffraction experiments. In Fig. 8, trace (a) is the input electrical signal of 1 kHz, trace

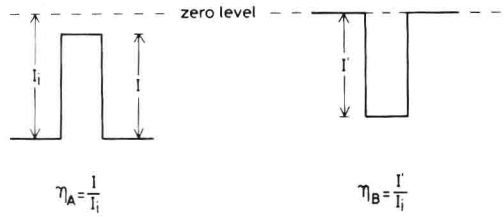

Fig. 7. The definition of two diffraction efficiencies η_A and η_B.

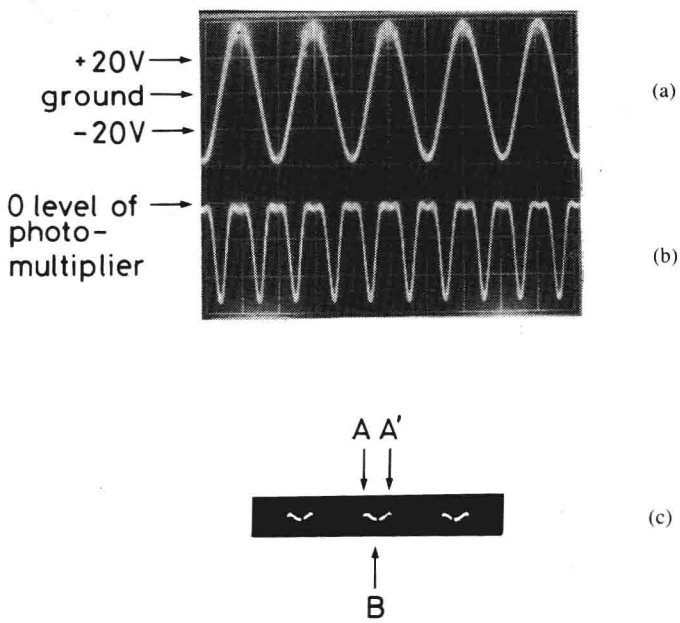

Fig. 8. Oscilloscope traces of the diffraction experiments. Trace (a) is for an input electrical signal of 1 kHz. Trace (b) is for the undiffracted beam corresponding to (a). Trace (c) is for the enlargement of a small portion of (b).

(b) is the corresponding undiffracted beam, and trace (c) is the enlargement of a small portion of (b). The marks A and A' correspond to the maximum diffraction efficiencies with respect to $+V_f$ and $-V_f$. Since the applied voltage at B is larger than the required applied voltage V_f for 100 percent diffraction, we can see very clearly from Fig. 8 that the diffraction efficiency becomes lower. If we increase the applied voltage more, we can expect the width between A and A' to increase.

Fig. 9 shows the diffraction efficiency η_A measurement of the sample A with a thickness of 1.03 μm using a dc power supply. The solid curve is $\sin^2 BV_0$ normalized to measured data at $\eta_A = 60$ percent. The data follow the sine-squared law, but with some rolloff at the higher voltage. The maximum diffraction efficiency is about 90 percent with an applied voltage of about 33.5 V. All of the measurements were made for the TE_0 mode at 6328 Å.

Fig. 10 shows the diffraction efficiency η_A measurement of the sample B with a thickness of 0.88 μm using a dc power supply. The solid curve is $\sin^2 BV_0$ normalized to measured data at $\eta_A = 60$ percent. The maximum efficiency η_A is about 95 percent with an applied voltage of about 28 V. It is still not very clear how the applied voltage corresponding to the maximum efficiency is related to

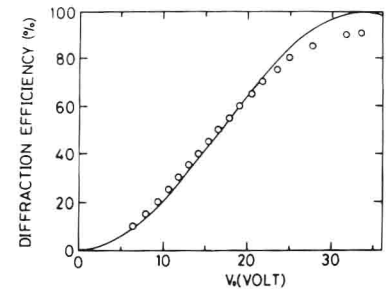

Fig. 9. Dependence of the diffraction efficiency η_A on applied voltage V_0 of sample A with a 1.03 μm thickness.

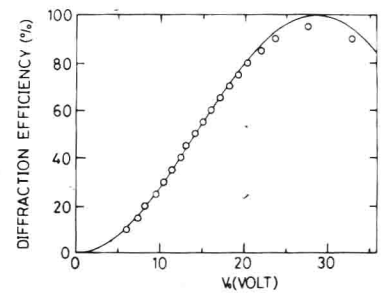

Fig. 10. Dependence of the diffraction efficiency η_A on applied voltage V_0 of sample B with a 0.88 μm thickness.

the thickness of the film. But it seems that V_f tends to be higher for those samples with larger thickness.

Fig. 11 shows our best diffraction efficiency η_A measurement, of the sample C with a thickness of 0.94 μm using a dc power supply. The solid curve is $\sin^2 BV_0$ normalized to measured data at $\eta_A = 70$ percent. The data follow the sine-squared law very well. The maximum diffraction efficiency η_A is about 98 percent at an applied voltage of about 31 V. The reproducibility is quite good.

The maximum efficiency is over 90 percent for almost all of the samples we made with thicknesses from 0.8 to 1.2 μm.

The resistivity of ZnO film after sputtering is about $10^6 \sim 10^7\ \Omega \cdot$ cm. But it decreases to $10^4 \sim 10^5\ \Omega \cdot$ cm after four months or half a year and becomes steady. There were no reports concerning any electrooptic diffraction modulation in ZnO film using a dc power supply. Hammer *et al.* [10] could not observe any diffraction of their ZnO thin film grating waveguide modulator with dc voltages applied.

The capacitance of the interdigital electrode we used is about 13 ~ 15 pF at 1 kHz, and the theoretical value is about 9 pF from (9). Based on this capacitance, the PPW factor of our device is about 20 mW/MHz. This value can be lowered much further, for example, by reducing the pair of interdigital electrodes and increasing the aperture or reducing the spatial period.

The low-frequency (unclamped) electrooptic coefficient r_{33} of ZnO film is calculated from (7) to be about 5.8×10^{-12} m/V, which is much larger than the clamped value of 2.6×10^{-12} m/V listed in the literature. There is no listed value of the unclamped electrooptic coefficient r_{33}

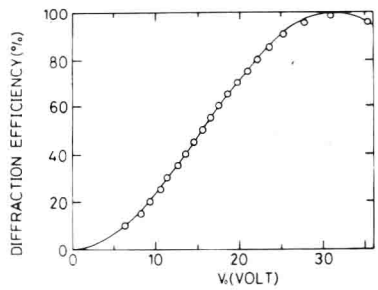

Fig. 11. Dependence of the diffraction efficiency η_A on applied voltage V_0 of sample C with a 0.94 μm thickness.

of ZnO in the literature. It is very interesting that there is such a large difference between the clamped and the unclamped r_{33} values of ZnO. The results are independent of the frequency in the range from dc to 100 kHz.

Since it is very lossy for the TM mode for our interdigital electrode fabricated directly on the ZnO film surface, we cannot measure the unclamped electrooptic coefficient r_{13} of ZnO. One solution to this is to sputter a very thin ($\sim$1500 Å) SiO_2 or Al_2O_3 buffer layer between the ZnO thin film and the interdigital electrode.

IV. Conclusion

The preparation of ZnO films on sapphire with an optical waveguide loss of about 0.5 dB $\cdot$ cm^{-1} has been obtained by the RF planar magnetron sputtering system. A maximum diffraction efficiency as high as 98 percent at 31 V for our ZnO electrooptic Bragg diffraction modulators has been obtained, with an optical waveguide and interdigital electrode integrated monolithically. To our knowledge, this is also the first report of the measurement of the unclamped electrooptic coefficient r_{33} of ZnO, which is estimated to be 5.8×10^{-12} m/V, with a frequency in the range from dc to 100 kHz.

References

[1] T. Shiosaki, "High-speed fabrication of high-quality sputtered ZnO thin films for bulk and surface wave applications," in *Proc. IEEE 1978 Ultrasonics Symp.*, 1978, pp. 100–110.

[2] T. Mitsuyu, S. Ono, and K. Wasa, "Structure and SAW properties of RF-sputtered single-crystal films of ZnO on sapphire," *J. Appl. Phys.*, vol. 51, pp. 2464–2470, May 1980.

[3] F. S. Hickernell, "Dc triode sputtered zinc oxide surface elastic wave transducers," *J. Appl. Phys.*, vol. 44, pp. 1061–1071, Mar. 1973.

[4] T. Shiosaki, E. Ieki, and A. Kawabata, "58-MHz surface-acoustic-wave video intermediate-frequency filter using ZnO-sputtered film," *Appl. Phys. Lett.*, vol. 28, pp. 475–476, May 1976.

[5] J. D. Larson, D. K. Winslow, and L. T. Zitelli, "RF diode sputtered ZnO transducers," *IEEE Trans. Sonics Ultrason.*, vol. SU-19, pp. 18–22, 1972.

[6] V. Jipson and C. F. Quate, "Acoustic microscopy at optical wavelengths," *Appl. Phys. Lett.*, vol. 32, pp. 789–791, June 1978.

[7] J. Kushibiki, H. Sasaki, N. Chubachi, N. Mikoshiba, and K. Shibayama, "Thickness dependence of acoustooptic diffraction efficiency in ZnO-film optical waveguides," *Appl. Phys. Lett.*, vol. 26, pp. 362–364, Apr. 1975.

[8] N. Chubachi, "ZnO films for acoustooptic devices on nonpiezoelectric substrates," *Proc. IEEE*, vol. 64, pp. 772–774, May 1976.

[9] J. M. Hammer, D. J. Channin, and M. J. Duffy, "Fast electrooptic waveguide deflector modulator," *Appl. Phys. Lett.*, vol. 23, pp. 176–177, Aug. 1973.

[10] J. M. Hammer, D. J. Channin, M. T. Duffy, and C. C. Neil, "High-speed electrooptic waveguide grating modulator using epitaxial ZnO," *IEEE J. Quantum Electron.*, vol. QE-11, pp. 138–148, Apr. 1975.

[11] J. M. Hammer, D. J. Channin, M. T. Duffy, and J. P. Witte, "Low-loss epitaxial ZnO optical waveguides," *Appl. Phys. Lett.*, vol. 21, pp. 358–360, Oct. 1972.

[12] E. L. Paradis and A. J. Shuskus, "RF sputtered epitaxial ZnO films on sapphire for integrated optics," *Thin Solid Films*, vol. 38, pp. 131–141, 1976.

[13] T. Shiosaki, S. Ohnishi, and A. Kawabata, "Optical properties of single crystalline ZnO film smoothly chemical-vapor deposited on intermediately sputtered thin ZnO film on sapphire," *J. Appl. Phys.*, vol. 50, pp. 3113–3117, May 1979.

[14] K. Setsune, T. Mitsuyu, and K. Wasa, "High-frequency AO Bragg deflector using a single-crystal ZnO thin film," in *Proc. 3rd Symp. Ultrasonics Electron.*, Tokyo, Japan; *Japan. J. Appl. Phys.*, vol. 22, suppl. 22-3, pp. 173–175, 1983.

[15] M.-S. Wu, T. Shiosaki, and A. Kawabata, "The refractive index measurements of RF magnetron sputtered ZnO thin film on sapphire," *IEEE J. Quantum Electron.*, vol. QE-23, pp. 1105–1107, July 1987.

[16] H. Jaffe and D. A. Berlincourt, "Piezoelectric transducer materials," *Proc. IEEE*, vol. 53, pp. 1372–1386, 1965.

[17] H. Sasaki, K. Tsubouchi, N. Chubachi, and N. Mikoshiba, "Photoelastic effect in piezoelectric semiconductor: ZnO," *J. Appl. Phys.*, vol. 47, pp. 2046–2049, May 1976.

[18] I. P. Kaminow and E. H. Turner, "Electrooptic light modulators," *Proc. IEEE*, vol. 54, pp. 1374–1390, Oct. 1966.

[19] R. C. Miller, "Optical second harmonic generation in piezoelectric crystals," *Appl. Phys. Lett.*, vol. 5, pp. 17–19, 1964.

[20] M.-S. Wu, A. Azuma, T. Shiosaki, and A. Kawabata, "Low-loss epitaxial ZnO optical waveguides on sapphire by RF magnetron sputtering," *J. Appl. Phys.*, vol. 62, pp. 2482–2484, Sept. 1987.

[21] D. Hall, A. Yariv, and E. Garmire, "Observation of propagation cutoff and its control in thin optical waveguide," *Appl. Phys. Lett.*, vol. 17, pp. 127–129, Aug. 1970.

[22] P. K. Tien, R. J. Martin, R. Wolf, R. C. Le-Craw, and S. L. Blank, "Switching and modulation of light in magnetooptic waveguides of garnet films," *Appl. Phys. Lett.*, vol. 21, pp. 394–396, Oct. 1972.

[23] W. R. Cook, Jr. and H. Jaffe, "Electrooptic coefficients," in Landolt-BörnsteinIII/11. Berlin, Heidelberg, New York: Springer-Verlag, 1979, pp. 552–651.

[24] W. R. Klein and B. D. Cook, "Unified approach to ultrasonic light diffraction," *IEEE Trans. Sonics Ultrason.*, vol. SU-14, pp. 123–134, July 1967.

[25] A. Yariv and P. Yeh, *Optical Waves in Crystals*. New York: Wiley, 1984, ch. 9, pp. 454–459.

[26] H. Engan, "Excitation of elastic surface waves by spatial harmonics of interdigital transducers," *IEEE Trans. Electron Devices*, vol. ED-16, pp. 1014–1017, Dec. 1969.

[27] Y.-K. Lee and S. Wang, "Electrooptic Bragg-deflection modulators: Theoretical and experimental studies," *Appl. Opt.*, vol. 15, pp. 1565–1572, June 1976.

[28] T. Shiosaki, S. Ohnishi, Y. Murakami, and A. Kawabata, "Higher rate epitaxial growth of ZnO films on sapphire by planar magnetron RF sputtering system," *J. Cryst. Growth*, vol. 45, pp. 346–349, Dec. 1978.

[29] G. A. Rozgonyi and W. J. Polito, "Epitaxial thin films of ZnO on CdS and sapphire," *J. Vac. Sci. Technol.*, vol. 6, pp. 115–119, Jan. 1969.

[30] S. Takada, M. Ohnishi, H. Hayakawa, and N. Mikoshiba, "Optical waveguides on single-crystal $LiNbO_3$ film deposited by RF magnetron sputtering," *Appl. Phys. Lett.*, vol. 24, pp. 490–492, May 1974.

[31] D. J. Channin, J. M. Hammer, and M. T. Duffy, "Scattering in ZnO-sapphire optical waveguides," *Appl. Opt.*, vol. 14, pp. 923–930, Apr. 1975.

[32] G. L. Tangonan, D. L. Persechini, J. F. Lotspeich, and M. K. Barnoski, "Electrooptic diffraction modulation in Ti-diffused $LiTaO_3$," *Appl. Opt.*, vol. 17, pp. 3259–3263, Oct. 1978.